Computer Science
Technical Report

Colorado State University

Echo State Networks for Modeling and Classification of EEG Signals in Mental-Task Brain-Computer Interfaces

Elliott M. Forney, Charles W. Anderson, William J. Gavin,
Patricia L. Davies, Marla C. Roll, Brittany K. Taylor

November 17, 2015

Colorado State University Technical Report CS-15-102

Computer Science Department
Colorado State University
Fort Collins, CO 80523-1873

Phone: (970) 491-5792 Fax: (970) 491-2466
WWW: http://www.cs.colostate.edu

Abstract

Constructing non-invasive Brain-Computer Interfaces (BCI) that are practical for use in assistive technology has proven to be a challenging problem. We assert that classification algorithms that are capable of capturing sophisticated spatiotemporal patterns in Electroencephalography (EEG) signals are necessary in order for BCI to deliver fluid and reliable control. Since Echo State Networks (ESN) have been shown to be exceptional at modeling non-linear time-series, we believe that they are well-suited for this role. Accordingly, we explore the ability of ESN to model and classify EEG recorded during several mental tasks. ESN are first trained to model EEG by forecasting the signals a single step ahead in time. We then take a generative approach to classification where a separate ESN models sample EEG recorded during each mental task. This yields a number of ESN that can be viewed as experts at modeling EEG associated with each task. Novel EEG data are classified by selecting the label corresponding to the model that produces the lowest forecasting error. An offline analysis was conducted using eight-channel EEG recorded from nine participants with no impairments and five participants with severe motor impairments. These experiments demonstrate that ESN can model EEG well, achieving error rates as low as 3% of the signal range. We also show that ESN can be used to discriminate between various mental tasks, achieving two-task classification accuracies as high as 95% and four-task accuracies as high as 65% at two-second intervals. This work demonstrates that ESN are capable of modeling intricate patterns in EEG and that the proposed classification algorithm is a promising candidate for use in BCI.

1 Introduction

Brain-Computer Interfaces (BCI) are emerging technologies that allow people to interact with computerized devices using only changes in mental state [1]. While BCI may eventually lead to many new forms of human-computer interaction, an important and immediately useful application is the development of assistive devices. Since those with limited motor function may find it difficult to interact through physical movement, BCI may be a useful alternative to mechanical input devices. For those with severe motor impairments that are progressive in nature, all other forms of assistive technology, such as eye trackers, switches and voice recognition, may eventually become ineffective. In these cases, even a BCI with a relatively slow communication rate may prove to be an invaluable tool and, potentially, a person's only method of communication [2, 3].

Among the approaches that have been proposed for constructing BCI, those that utilize scalp-recorded Electroencephalography (EEG) appear to be particularly promising [4, 5]. Since EEG is non-invasive, users are not required to undergo surgical procedures and researchers are free to investigate new methods with minimal risk. Although EEG suffers from a low signal-to-noise ratio and moderate spatial resolution, its high temporal resolution and history of successful use in BCI are redeeming [4–6]. Furthermore, EEG hardware is relatively inexpensive and can be contained in a portable system. Overall, it appears that EEG is well-suited for use in many types of BCI.

In a number of studies, EEG-based BCI that combine mental-task communication paradigms with techniques from machine learning have shown considerable potential [7–24]. When using a mental-task communication paradigm, a user issues instructions to the BCI by performing one of several predetermined mental tasks. For example, a user might imagine making a fist in order

to move a cursor to the left or silently sing a song to move it to the right. Mental-task communication paradigms allow tasks involving visualization, language, analytical thinking, music and motor imagery to be combined in a way that is user-friendly while also eliciting diverse changes in EEG across various brain regions [7, 18, 25, 26]. When combined with machine learning, these BCI may have the potential to attain several degrees of control and a high level of adaptability on the part of the user as well as the BCI.

Nevertheless, constructing practical BCI that use EEG and mental-task paradigms has proven to be a challenging problem for several reasons. First, the sheer complexity of the human brain suggests that EEG signals likely contain sophisticated spatiotemporal patterns. Second, there does not appear to be any single type of change in EEG that can universally be used to discriminate between mental tasks. Third, the patterns in EEG that are associated with mental tasks can vary considerably among different BCI users and over the course of time. Finally, the noisy nature of EEG and the fact that humans are continually performing multiple simultaneous tasks means that desirable signal components are often masked by noise, artifacts and background mental activity. We assert that carefully designed machine learning algorithms and signal processing techniques are required in order to overcome these challenges and develop BCI that are capable of delivering reliable and fluid control at a rapid pace.

A number of machine learning algorithms have been proposed for filling this role. For instance, Millán, et al. [20–22], Galán, et al. [23], and Zhiwei, et al. [24], have explored the use of frequency-domain signal representations constructed from Fourier and Wavelet Transforms in combination with various classifiers and feature selection algorithms. Although frequency-domain representations may be well-suited for capturing periodic patterns in EEG, they often suffer from a limited ability to capture non-stationary and short-term patterns. These methods also do not typically consider spatial patterns in the form of phase differences across channels.

Approaches proposed by Anderson, et al. [10–13], and Friedrich, et al. [18, 19], combine time-delay embedding with various classifiers and linear transforms for dimensionality reduction. Time-delay embedding is capable of capturing spatiotemporal patterns; however, the length of temporal information is limited by the size of the embedding dimension and a large embedding dimension can lead to a high-dimensional feature space. Although linear transforms and source separation techniques appear promising for dimensionality reduction, selecting desirable components can be challenging and automated techniques have not been adequately explored [27].

An alternative to these approaches that may be able to capture spatiotemporal patterns while avoiding high-dimensionality involves the use of predictive models. Along these lines, Keirn and Aunon [7] as well as Anderson, et al. [8, 9], have applied several types of classifiers to the coefficients resulting from linear Autoregressive (AR) models. Subsequently, Coyle, et al. [14], suggested that applying a classifier to the residuals from forecasting models that utilize non-linear feedforward networks and time-delay embedding may outperform linear AR models. Coyle, et al. [28–32], have also proposed several other methods that use predictive models to filter and derive features for BCI.

In our previous work, we have begun to explore the use of errors resulting from forecasting EEG with Recurrent Neural Networks (RNN), i.e., networks with feedback connections [15–17]. Since RNN can model non-linear processes and because they have an intrinsic state and memory, we believe that they may be better-suited for modeling EEG than linear AR models and feedforward networks.

In the present study, we extend our work by exploring the ability of Echo State Networks (ESN) to model and classify EEG within the framework of mental-task BCI. ESN are a type of RNN that rely on a large, sparsely connected reservoir of artificial neurons that are tuned only during the initialization process. A linear readout layer is then trained to map the reservoir activations

to outputs using a straightforward linear regression. This optimization scheme allows ESN to be trained quickly, making them suitable for use in interactive BCI. Furthermore, several recent studies have demonstrated that ESN perform favorably on a number of non-linear dynamical systems modeling and control problems [33–35].

In order to exploit the apparent potential for ESN to capture patterns in EEG, we propose a generative classifier. In this approach, ESN are first trained to model EEG by forecasting the signal a single step ahead in time. Separate models are trained over sample EEG recorded during each of several mental tasks. Each ESN can be thought of as an expert at modeling EEG associated with a given mental task. These models are then leveraged to label novel EEG by applying each ESN to the signal and assigning the class label associated with the model that produces the lowest forecasting error.

In Section 2, we begin by describing the participants, experimental protocol, EEG acquisition hardware and preprocessing methods used to construct the dataset examined throughout this manuscript. In Section 3, we continue by giving a thorough description of our rendition of ESN as well as the methods that we have used to tune the various parameters involved. In Section 4, we investigate the ability of ESN to forecast EEG signals and examine the relationship between our regularization parameters and the complexity of our models. In Section 5, we formalize our approach to EEG classification and present the final outcomes of our classification experiments. Finally, in Section 6, we perform a cursory comparison with other approaches, provide some concluding remarks and offer potential directions for future research.

2 Participants and Data Collection

In the present study we examine a BCI dataset that we have collected for offline analysis.[1] This dataset was acquired using a g.tec g.MOBILab+ with g.GAMMASys active electrodes. This system features eight active electrodes that were placed laterally at sites F3, F4, P3, P4, C3, C4, O1 and O2 according to the 10/20 system, depicted in Figure 1. This channel arrangement was designed to cover a wide variety of cortical regions in each hemisphere of the brain using the eight available electrodes. The g.MOBILab+ also has an active hardware reference that was linked to the right earlobe and a passive ground that was placed at site FCz. This system has a sampling frequency of 256Hz and a hardware bandpass filter from 0.5–100Hz at -3dB attenuation. The g.MOBILab+ is lightweight, battery-powered and communicates via a bluetooth transceiver. Although this system offers relatively few channels and a low sampling rate, we believe that its portability and ease-of-use make it representative of the types of EEG systems that are likely to be used in practical BCI [36].

Several preprocessing steps were carried out in software in order to reduce noise and artifacts. First, a third order, zero-phase Butterworth highpass filter with a cutoff at 4Hz was applied in order to reduce slow drift and artifacts caused by ocular movement. A stopband filter with similar characteristics was then applied to the 59–61Hz band in order to eliminate interference induced by external power mains and equipment. Next, a common-average reference was applied in order to attenuate signals and interference common to all channels. Finally, each channel was standardized to have zero mean and unit variance using the sample mean and variance from the relevant training partition. This standardization procedure ensures that the signals for each channel have roughly the same scale and prevents the errors produced by our forecasting models from being dominated by a single channel. A pilot study involving the validation data for the first five participants supports our use of these preprocessing steps.

[1] This dataset is publicly available at `http://www.cs.colostate.edu/eeg`.

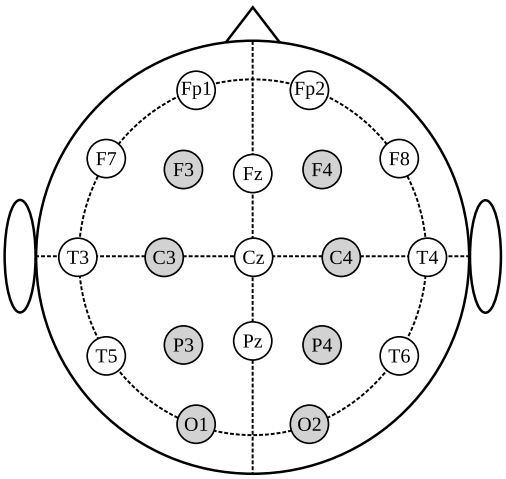

Figure 1: Eight-channel subset of the 10/20 system used for EEG acquisition. The channels used are shown in gray.

Data were collected from a total of 14 participants. Nine participants had no known medical conditions and EEG recording took place in the Brainwaves Research Laboratory in the College of Health and Human Sciences at Colorado State University [37, 38]. This group is intended to represent the best-case scenario for a BCI user by minimizing interference from environmental noise sources and by avoiding other potential challenges that might arise when recording EEG from those with motor impairments. The remaining five participants had severe motor impairments, three with progressive multiple sclerosis and two with quadriplegia due to high-level spinal cord injuries. For this group, EEG recording took place in each participant's home environment in order to closely replicate realistic operating conditions for an assistive BCI.

Table 1: Mental tasks used and cues shown to the participants.

Cue	Task description
Song	Silently sing a favorite song.
Fist	Imagine repeatedly making a left-handed fist.
Rotate	Visualize a cube rotating in three-dimensions.
Count	Silently count backward from 100 by threes.

Following the application of the EEG cap, each participant was positioned comfortably in front of a computer screen and instructed to perform one of four mental tasks during a visual cue in the form of a single word, summarized in Table 1. All data collection and cue presentation was performed using custom software [39]. Participants were asked to perform each task consistently and repeatedly during the cue. They were also asked to move as little as possible and to blink as infrequently as comfort allowed. Each cue was presented on the screen in a random order for 10 seconds during which the participant was instructed to perform the corresponding task. A blank screen was then presented for five seconds during which the participant was instructed to relax. Each participant performed a single practice trial after which they were al-

lowed to ask the operator questions. After the practice trial, five additional trials were performed yielding 50 seconds of data per mental task totaling 200 seconds of usable EEG per participant. Participants 9 and 13 were exceptions to this, having only completed four trials due to a battery failure and procedural error, respectively. The EEG data were then split into two-second segments for our classifiers to label, yielding 25 segments per mental task for a total of 100 EEG segments per participant. Our choice of a two-second interval is supported by our previous research [16], which suggests that assigning class labels at a rate of 0.5–1 instructions-per-second leads to a high information transfer rate while not exceeding the rate at which a BCI user can be reasonably expected to send instructions to the system.

The EEG segments for each participant were then divided into a 60% partition for training and 40% for testing generalization performance. All model tuning and parameter selection was performed using a five-fold cross validation over the training partition. Final test performance was evaluated by training the model over the entire training partition using the parameters found during cross-validation and then observing the performance of the model on the unused test partition.

3 Echo State Networks

Echo State Networks (ESN) are a type of artificial neural network originally proposed by Herbert Jaeger and with an international patent held by the Fraunhofer Institute for Intelligent Analysis [33, 34, 40]. ESN have several properties that may be beneficial for capturing patterns in EEG. First, ESN have recurrent connections that give them memory and the ability to incorporate information from previous inputs. This allows ESN to capture temporal patterns without using frequency-domain representations or explicitly embedding past signal values. Second, ESN are easily extended to the multivariate case and typically include sigmoidal transfer functions, allowing them to capture non-linear spatiotemporal relationships. Third, ESN have several parameters that can be used to limit the complexity of the network. This allows ESN to be regularized in a way that may be robust to noise, artifacts and background mental activity. Finally, ESN can be trained and evaluated quickly on commodity computing hardware, making real-time applications feasible.

3.1 Architecture

ESN have a two-layer architecture, depicted in Figure 2. The first layer, termed the reservoir, consists of artificial neurons with sigmoidal transfer functions. The neurons in the reservoir have weighted connections from the network inputs as well as weighted recurrent connections with a single-timestep delay. The second layer, termed the readout, consists of neurons with feedforward connections and linear transfer functions.

Consider an ESN with L inputs, M reservoir neurons and N outputs. The network inputs can then be thought of as a multivariate function of time with $\mathbf{x}(t)$ denoting an $L \times 1$ column vector of signal values at time t. The reservoir output, also known as the network context, is then the $M \times 1$ column vector

$$\mathbf{z}(t) = \tanh(\mathbf{H}\bar{\mathbf{x}}(t) + \mathbf{R}\mathbf{z}(t-1)) \tag{1}$$

where $\mathbf{H}$ is the $M \times (L+1)$ adjacency matrix of feedforward weights into the reservoir and $\mathbf{R}$ is the $M \times M$ matrix of recurrent weights. Note that a bar over a matrix denotes that a row of ones has been appended for a bias term. We choose to use the hyperbolic tangent transfer function, denoted $\tanh$, because it is symmetrical, fast to compute and commonly used in ESN.

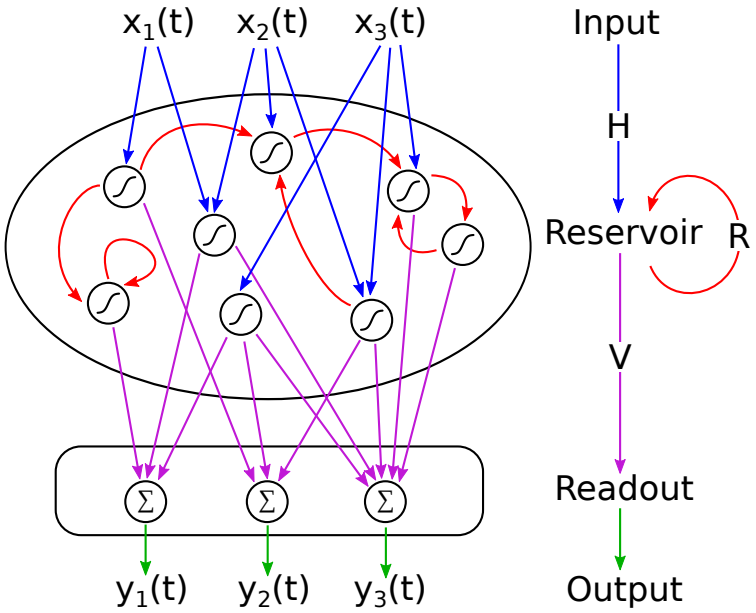

Figure 2: The architecture of an Echo State Network with inputs $\mathbf{X}$, input weights $\mathbf{H}$, recurrent weights $\mathbf{R}$, readout weights $\mathbf{V}$ and outputs $\mathbf{Y}$.

The final output of the network at time t is then the $N \times 1$ column vector

$$\mathbf{y}(t) = \mathbf{V}\bar{\mathbf{z}}(t) \tag{2}$$

where $\mathbf{V}$ is the $N \times (M+1)$ matrix of weights for the readout layer. For the sake of notational brevity, we write the network output at time t as

$$\mathbf{y}(t) = esn(\mathbf{x}(t)). \tag{3}$$

3.2 Training and Parameter Tuning

The primary difference between ESN and many other types of recurrent networks is that the reservoir weight matrices, $\mathbf{H}$ and $\mathbf{R}$, are not optimized during the training procedure. Instead, they are chosen in a semi-random fashion that is designed to yield a large number of diverse reservoir activations while also achieving the Echo State Property (ESP). Briefly stated, a reservoir is said to possess the ESP if the effect on the reservoir activations caused by a given input fades as time passes. The ESP also implies that the outputs produced by two identical ESN will converge toward the same sequence when given the same input sequence, regardless of the starting network context.

In order to achieve these properties, we follow a modified version of the guidelines suggested by Jaeger [33]. First, the feedforward weights into the reservoir, $\mathbf{H}$, are chosen to be sparse with 80% of the weights being zero. Sparsity is intended to improve the diversity of the reservoir activations by reducing the effect of any single input on all of the reservoir neurons. The remaining weights are selected from the random uniform distribution between $-\alpha$ and α.

Typically, α is chosen empirically through trial and error. We take this a step further by asserting that the value of α should be selected in a way that limits the saturation of the $\tanh$ reservoir transfer function. This is done by taking a sample EEG signal and examining the distribution of

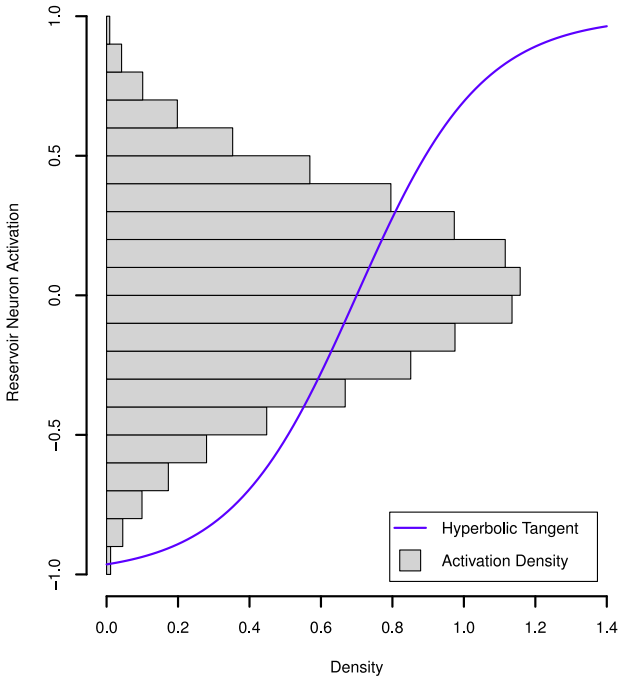

Figure 3: Histogram of reservoir activations and the hyperbolic tangent for $\alpha = 0.35$ and $\lambda = 0.6$ and $N = 1000$ for sample EEG. The majority of activations do not lie in the saturated regions of $\tanh$.

the reservoir activations over the hyperbolic tangent. We illustrate this in Figure 3 by superimposing the hyperbolic tangent over a histogram of the reservoir activations generated from the training EEG for Participant 1 when $\alpha = 0.35$. In this case, the vast majority of activations lie on the near-linear and non-linear regions near the center while few activations fall on the saturated regions at the tails. Although this distribution changes somewhat as other network parameters vary, we find that a value of $\alpha = 0.35$ works well in the current setting.

Next, our initial recurrent reservoir weights, $\mathbf{R}_0$, are also chosen to be sparse with 99% of the weights being zero and with the remaining weights selected from a random uniform distribution between -1 and 1. In order to achieve the ESP, $\mathbf{R}_0$ is then scaled to have a spectral radius, i.e., magnitude of the largest eigenvalue, of less than one. Although this is not a sufficient condition for the ESP, it appears that reservoirs constructed using this method typically achieve the ESP in practice [33]. If λ_0 is the spectral radius of $\mathbf{R_0}$, then our final recurrent weight matrix is

$$\mathbf{R} = \frac{\lambda}{\lambda_0}\mathbf{R}_0 \tag{4}$$

where λ is the desired spectral radius. Since λ determines the rate at which information fades from the reservoir, we view it as a regularization parameter that limits the temporal information included in our models. Effective values for λ are empirically determined on an individual basis and are thoroughly explored in Sections 4.1 and 5.1.

We have explored the use of various reservoir sizes in each of our experiments. From these trials we have concluded that reservoirs consisting of $M = 1000$ neurons consistently generate good results. Although reservoirs with as few as 200 neurons can work well, larger reservoirs appear to deliver more consistent results across both weight initializations as well as across dif-

ferent participants. This conclusion seems reasonable since larger reservoirs generate a wider variety of activations for the readout layer to utilize while smaller reservoirs generate less diverse activations. In other words, smaller reservoirs depend more heavily on a good random weight initialization.

In all of the experiments presented here, we have elected to use a single reservoir initialization, i.e., weight selection for $\mathbf{H}$ and $\mathbf{R}_0$. These matrices were chosen empirically during a small pilot study involving five randomly chosen reservoirs and the validation partitions from the first five participants. However, the difference in performance across reservoirs was very slight, typically less than 1% difference in classification accuracy. Given the consistency we have observed across large reservoirs, we suspect this to be true in general. Furthermore, using a single initial reservoir ensures that our models are as comparable as possible and leads to better computational efficiency through the reuse of reservoir activations.

At any given time, the temporal information contained in an ESN is stored in the context vector $\mathbf{z}$. In order to start our ESN with a reasonable state, we follow the common practice of initializing the context vector to $\mathbf{z}(0) = \mathbf{0}$ and then allowing the reservoir to run for an initial transient period of $\rho = 64$ timesteps before using any of the reservoir outputs for further processing. Since our sampling frequency is 256Hz, this is equivalent to $\frac{1}{4}$ of a second of EEG. This transient period allows the network to acclimate to the input signal and for the effects of the initial context vector to fade.

Finally, the weights in the readout layer of our ESN are optimized using a closed-form linear least-squares regression. This is possible because the transfer function in the readout layer is linear and because the weights of the reservoir are fixed. We also incorporate a ridge regression penalty, γ, that can be used to regularize the readout layer by pulling the weights of $\mathbf{V}$ toward zero. This may improve generalization by encouraging the readout layer to have a small reliance on a wide variety of reservoir neurons.

More formally, let T be the number of timesteps in our training signal and $\mathbf{A}$ be the $M \times T$ matrix of reservoir activations produced by concatenating the columns of $\mathbf{z}(t)$ for $t = 1, 2, \ldots, T$. Next, let $\mathbf{G}$ be the $N \times T$ matrix of target outputs produced by concatenating the columns of the desired outputs of the ESN. The weights for the readout layer are then

$$\mathbf{V} = \mathbf{G}((\bar{\mathbf{A}}\bar{\mathbf{A}}^{\mathsf{T}} + \mathbf{\Gamma})^{*}\bar{\mathbf{A}})^{\mathsf{T}} \tag{5}$$

where * denotes the Moore-Penrose pseudoinverse and $\mathbf{\Gamma}$ is a square matrix with the ridge regression penalty, γ, along the diagonal except with a zero in the last entry to avoid penalizing the bias term. Since γ is viewed as a regularization parameter, appropriate values are determined empirically in Sections 4.1 and 5.1.

4 Forecasting

Now that we have described our methods for training and evaluating ESN, we proceed by exploring the ability of these networks to model EEG. This is achieved by training ESN to forecast EEG signals a single step ahead in time. Our network inputs are then $\mathbf{x}(t) = \mathbf{s}(t)$ and the target outputs are $\mathbf{g}(t) = \mathbf{s}(t+1)$ for $t = 1, 2, ..., T-1$ where $\mathbf{s}(t)$ is the column vector of EEG signal voltages at time t and where T is the total number of timesteps in the training signal. The scalar sum-squared forecasting error accumulated over the length of the signal and across all channels is then

$$\xi = \sum_{t=1}^{T-1} \sum_{n=1}^{N} [y_n(t) - g_n(t)]^2 \tag{6}$$

where $N = 8$ is the number of EEG channels.

We also provide a baseline metric that is designed to help us evaluate our forecasting models. Referred to as the naive error, this metric is the sum-squared forecasting error that would be obtained if the model simply repeats the previous signal value. The naive error can be written as

$$\xi_0 = \sum_{t=1}^{T-1} \sum_{n=1}^{N} [s_n(t) - s_n(t+1)]^2 . \tag{7}$$

Ideally, the naive error should be an upper bound on the forecasting error obtained by a model that is able to learn meaningful patterns in the signal.

In order to present a more intuitive measure of forecasting error, we present our final results as a percent of signal range using the normalized root-mean-squared error (NRMSE),

$$NRMSE = \frac{100}{signal\ max - signal\ min} \sqrt{\frac{\xi}{N\ (T-1)}}. \tag{8}$$

4.1 Forecasting Regularization

Now that we have established methods for modeling EEG signals and quantifying the resulting errors, we continue by examining how our regularization parameters affect forecasting performance. In Figure 4, we show how the training and validation NRMSE for Participant 4 change as we vary the spectral radius and ridge regression penalty. These figures are representative of the regularization process for all 14 participants.

Not surprisingly, the lowest training NRMSE is encountered when our regularization parameters impose little or no limitation on our model complexity, i.e., with a spectral radius near one and a ridge regression penalty near zero. The lowest validation NRMSE, on the other hand, is typically achieved with a spectral radius near one and a moderate ridge regression penalty.

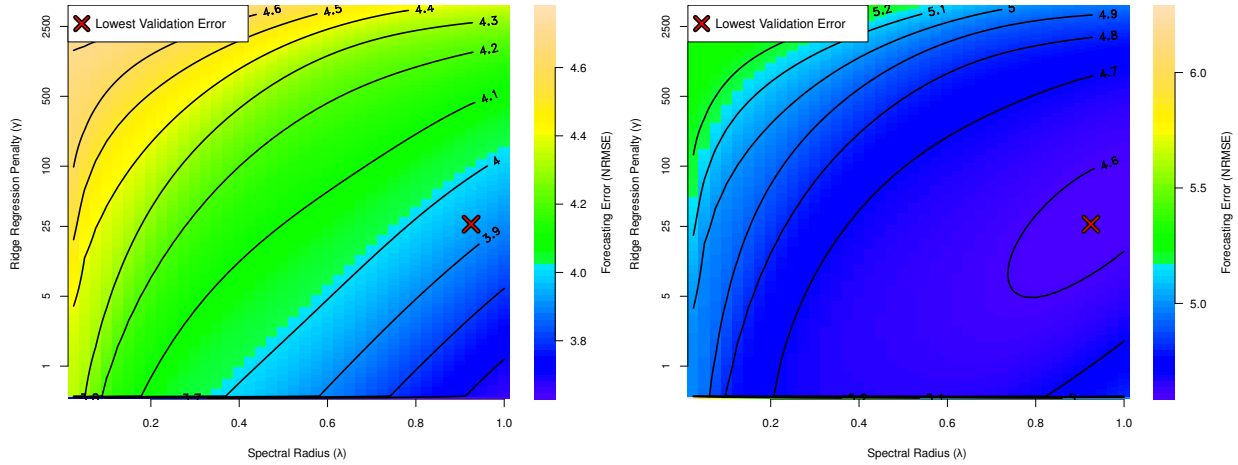

(a) Training NRMSE.

(b) Validation NRMSE.

Figure 4: Training and validation forecasting NRMSE for Participant 4 as the spectral radius and ridge regression penalty are varied. The lowest errors are typically achieved with a high spectral radius. A moderate ridge regression penalty yields the best generalization.

Combined, these results suggest that our ESN forecasting models are able to overfit EEG signals and that tuning our regularization parameters improves generalization. In particular, it appears that a conservative ridge regression penalty is effective at limiting overfitting by encouraging small weights in the readout layer. However, the fact that models with a relatively high spectral radius often generalize the best indicates that longer-term temporal information is useful for forecasting and that limiting the length of temporal information included in our models is not usually effective at preventing overfitting, at least in the sense of forecasting errors.

4.2 Forecasting Performance

Next, we examine the final performance of our models in terms of forecasting NRMSE alongside our benchmark naive NRMSE. In Table 2, we show both the naive and test forecasting NRMSE for each participant along with the individual values of our regularization parameters, λ and γ, found using the validation procedure described in Sections 2 and 4.1. Table 2 also shows the mean NRMSE and 95% confidence intervals, derived using the t-distribution, for both the group of participants with no motor impairments in the laboratory as well as for the group of participants with motor impairments in their homes.

Table 2: Average forecasting NRMSE across all four tasks.

	Participant	Naive NRMSE	Test NRMSE	λ	γ
No Impairment	1	6.8	5.9	1.0	125.9
	2	7.4	6.4	1.0	190.5
	3	4.6	4.1	1.0	151.4
	4	4.4	3.7	0.9	26.3
	5	5.9	5.0	0.8	63.1
	6	5.2	4.5	1.0	47.9
	7	6.4	5.6	1.0	125.9
	8	7.3	6.5	1.0	251.2
	9	6.3	5.4	0.6	41.7
	Mean	6.0 ± 0.8	5.2 ± 0.8		
Impairment	10	6.2	5.2	0.8	109.6
	11	3.8	3.0	0.9	21.9
	12	13.8	4.5	1.0	2.5
	13	5.7	4.4	0.8	20.0
	14	5.3	4.5	1.0	316.2
	Mean	6.9 ± 4.9	4.3 ± 1.0		

For every participant, the ESN models are able to outperform the naive solution, achieving forecasting NRMSE between 3.0–6.5% of the signal range. Note that the unusually high naive NRMSE for Participant 12 appears to be caused by a large amount of high-frequency noise on channel P3 during the later part of the recording session, potentially due to an electrode becoming dislodged. A paired two-sided t-test shows a statistically significant difference between the mean of the naive and test forecasting NRMSE for the group of participants without motor impairments ($p = 3.1 \times 10^{-7}$). For the smaller group of participants with motor impairments, we do not find a statistically significant difference between the mean naive and test NRMSE ($p = 0.19$).

We do, however, arrive at a significant difference among the users with motor impairments if we exclude Participant 12 ($p = 4.6 \times 10^{-3}$). These results suggest that ESN are able to learn meaningful patterns in EEG that allow them to forecast the signal better than a single-timestep shift.

4.3 Iterated Models

In order to gain further insight into the patterns learned by our forecasting models, we also investigate the effects of placing a feedback loop from the output of a trained ESN back to the network's inputs. This forms an autonomous, self-driven system known as an iterated model. These models may help illustrate the temporal behavior and internal dynamics of our forecasting models.

In order to construct an iterated model, we first train an ESN to forecast eight seconds of EEG. After the eight-second mark is reached, the network begins to use its past predictions as input, instead of the true EEG. Over the course of the experiment, the output of the ESN can be described by the recurrence relation

$$\mathbf{y}(t) = \begin{cases} \mathit{esn}(\mathbf{s}(t-1)), & \text{if } t < 8 \cdot 256 \\ \mathit{esn}(\mathbf{y}(t-1)), & \text{otherwise,} \end{cases} \tag{9}$$

where $\mathbf{s}(t)$ is the true EEG signal at time t and 256 is the sampling frequency.

In Figure 5, we show an instance of this experiment two-seconds before and after the transition to an iterated model as the spectral radius, λ, is varied. Although all eight EEG channels were used by the model, only channel P4 is shown for the sake of clarity. We note that these results are largely representative of other channels and can be reproduced, with a degree of variation, across reservoir initializations. With a relatively small spectral radius, less than about 0.4, the output of our iterated model quickly dampens to zero. With a mid-range spectral radius, around 0.7, the output of our iterated model oscillates indefinitely with a predominant frequency that is typically between 8–14Hz. As the spectral radius approaches one, our iterated model begins to produce a sophisticated signal that appears to be similar to the true EEG.

In order to support our claim that iterated models with a large spectral radius produce output similar similar to true EEG, we also examine energy spectra generated using continuous wavelet transforms. In Figure 6a we show the energy spectrum of the same true EEG signal that is shown in Figure 5. In Figure 6b, we show the energy spectrum of the signal produced by our iterated model with a unit spectral radius, which is also shown in Figure 5c. Again, the forecasting model is shown before the eight-second mark and the output of the iterated model is shown afterward. Although the two clearly differ, both signals appear to have similar transient changes in energy content across the frequency spectrum.

Although our forecasting models ultimately use only single-step-ahead predictions, our experiments with iterated models lead us to several important conclusions. First, a small spectral radius leads to models that include only very short-term temporal information. As the spectral radius increases, the model becomes increasingly influenced by the more predominant oscillatory components of the EEG signal. As the spectral radius approaches one, the ESN begins to model high-frequency information as well as non-periodic and non-stationary dynamics. Finally, we believe that these experiments demonstrate that ESN are able to learn sophisticated long-term patterns found in EEG.

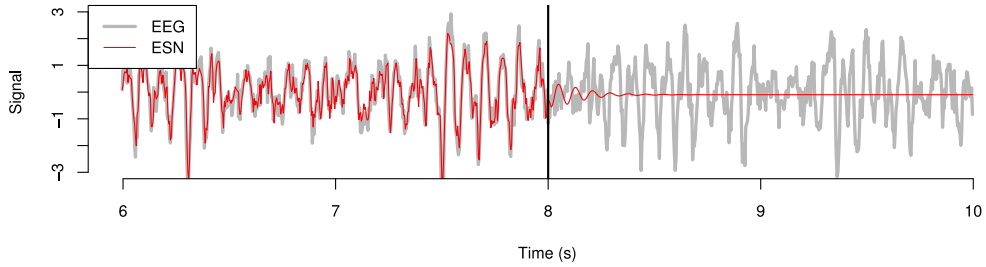

(a) Iterated model with $\lambda = 0.4$

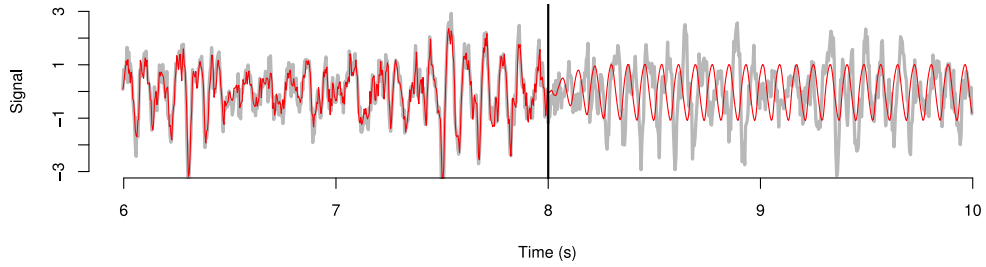

(b) Iterated model with $\lambda = 0.7$

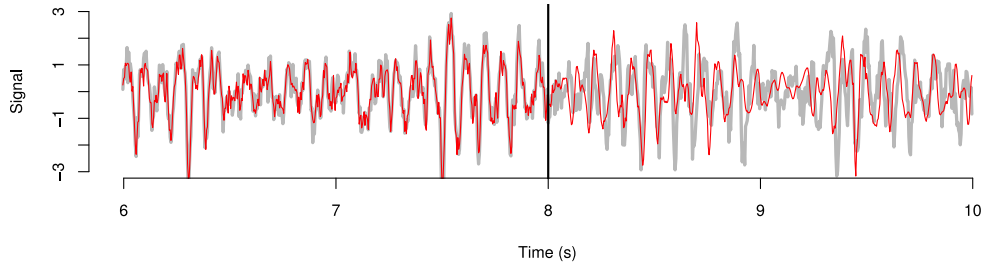

(c) Iterated model with $\lambda = 1.0$

Figure 5: A trace illustrating an ESN transitioning from forecasting to an iterated model at the eight-second mark. 5a) With a small spectral radius, the signal quickly dampens to zero. 5b) With moderate spectral radius, the signal oscillates indefinitely with a frequency of about 12Hz. 5c) With a large spectral radius, the signal exhibits sophisticated dynamics similar to the true EEG.

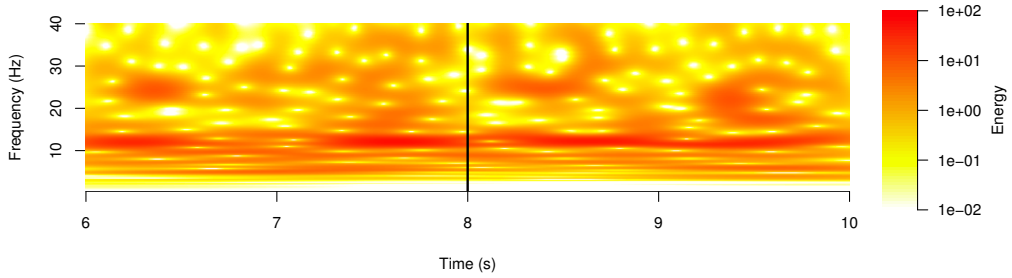

(a) Energy spectrum of true EEG.

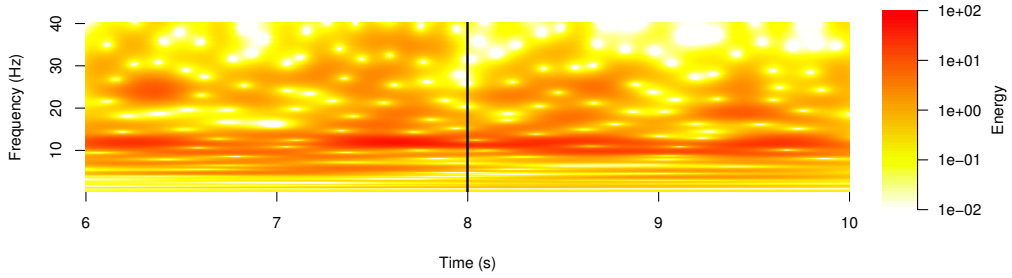

(b) Energy spectrum of ESN output.

Figure 6: Energy spectra of an ESN transitioning from forecasting to an iterated model at the eight-second mark. 6a) The energy spectrum of the true EEG. 6b) The energy spectrum of the ESN output. The ESN is forecasting before eight seconds and an iterated model afterward.

5 Classification

Now that we have demonstrated the ability of ESN to forecast EEG signals, we proceed by leveraging these models to construct EEG classifiers for use in BCI. In order to achieve this, we take a generative approach. First, a separate ESN is trained to forecast sample EEG recorded during each mental task. For a BCI that utilizes K different mental tasks, K different ESN are trained. We then have an ESN associated with each mental task that can be viewed as an expert at forecasting the corresponding EEG signals.

Once these models are trained, previously unseen EEG is labeled by applying each ESN and selecting the class label associated with model that best fits the signal. We achieve this by first measuring the sum-squared forecasting error, as described in (6), for each ESN. The final class label C is then

$$C = \underset{k\in\{1,2,\ldots,K\}}{\operatorname{argmin}} \ \xi_k \tag{10}$$

where ξ_k is the sum-squared forecasting error produced by the ESN trained to forecast the mental task indexed by k and where K is the total number of mental tasks used. Although a secondary classifier could potentially be used to assign class labels by using these forecasting errors as features, we have found that this best-fit approach typically works well without introducing additional parameters [16].

In order to describe our results in a way that can be compared with other studies and that conveys the type of experience that a BCI user might have, we use two classification performance metrics. First, we report classification accuracy (CA) as percent correct classification at two-second intervals. Although CA characterizes how often the classifier is correct, it can be misleading because it does not take into account how many classes were used and the rate at

which class labels are assigned. For these reasons, we also report information transfer rate (ITR) in bits-per-minute (bpm). We use the formulation of ITR that was adapted for use in BCI by Wolpaw, et al. [41], using the work in information theory done by Pierce [42]. This definition of ITR can be written as

$$ITR = V\left(\log_2 K + P\log_2 P + (1-P)\log_2\frac{1-P}{K-1}\right) \tag{11}$$

where $V = 30$ is the classification rate in decisions per minute, K is the number of classes and P is the fraction of correct decisions over the total decisions made.

5.1 Classifier Regularization

Now that we have formalized our classifier, we continue by exploring how our regularization parameters affect classification performance. Although we have established values for the spectral radius and ridge regression penalty that achieve low forecasting errors, the same parameters may not work well for classification. This is because noisy or undesirable components of an EEG signal may be highly predictable in the sense of forecasting while not carrying information that is useful for discriminating between mental tasks.

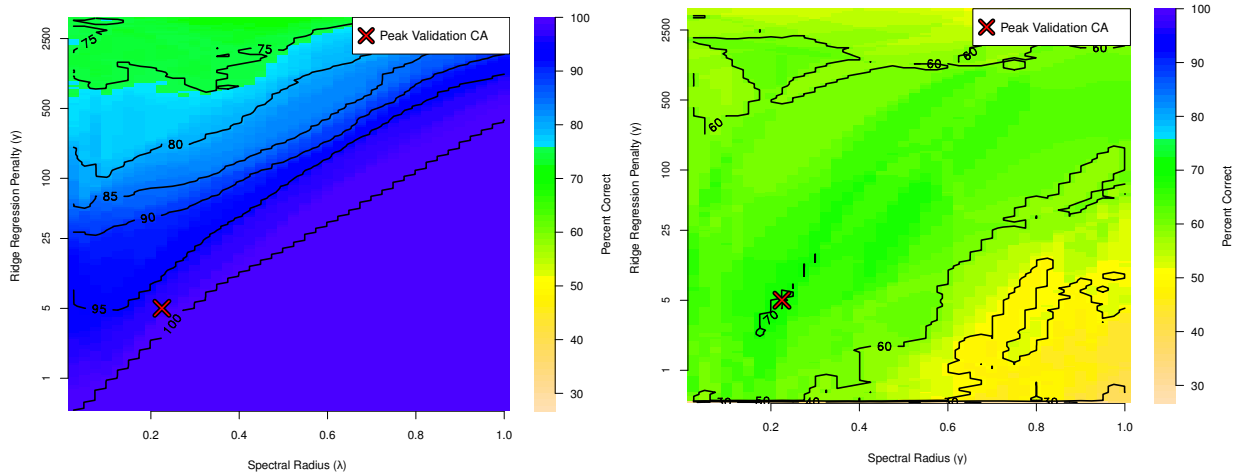

(a) Training accuracy.

(b) Validation accuracy.

Figure 7: Training and validation classification accuracy for Participant 1 as the spectral radius and ridge regression penalty are varied. Validation accuracy peaks near the contour where the training accuracy nears 100%, suggesting that overfitting is limited.

In Figure 7, we show the training and validation classification accuracies for Participant 1 as the spectral radius and ridge regression penalty are varied. In this instance, we note that the values for the spectral radius that produce the best validation classification accuracy are considerably smaller than those that produce the lowest forecasting error. This suggests that some of the more complex patterns that aid in forecasting are not helpful in discriminating between mental tasks. We also notice that the best validation accuracy tends to occur along the contour where training accuracy nears 100% correct. This suggests that our regularization parameters

are limiting overfitting by preventing our models from precisely fitting the data in the training partition. It is important to note, however, that the topography of these experiments varies considerably among the participants in our dataset.

5.2 Classifier Performance

Now that we have fully described our framework for using ESN to model and classify EEG, we report our final classification results. First, we apply our classification algorithm to all four mental tasks for each of our 14 participants. Class labels are assigned at non-overlapping two-second intervals. Suitable values for our regularization parameters, λ and γ, are found on an individual basis using the procedures described in Sections 2 and 5.1. The final outcomes of these experiments are displayed in Table 3, which includes training, validation and test classification accuracies as well as test information transfer rates and the final values of our regularization parameters. The mean of our performance metrics along with 95% confidence intervals are also reported for both groups of participants.

Table 3: Four-task performance results.

	Participant	Training CA (%)	Validation CA (%)	Test CA (%)	Test ITR (bpm)	λ	γ
No Impairment	1	97.5	71.7	62.5	13.5	0.2	5.0
	2	100.0	50.0	42.5	3.1	0.8	1.0
	3	92.1	53.3	55.0	8.8	0.2	95.5
	4	100.0	68.3	65.0	15.3	0.8	8.7
	5	98.8	46.7	45.0	4.1	0.2	0.7
	6	100.0	71.7	62.5	13.5	0.5	0.7
	7	88.8	55.0	40.0	2.3	1.0	3467.4
	8	100.0	68.3	62.5	13.5	0.6	41.7
	9	74.5	65.0	53.1	7.8	0.1	69.2
	Mean	94.6 ± 6.6	61.1 ± 7.6	54.2 ± 7.4	9.1 ± 3.9		
Impairment	10	92.9	51.7	27.5	0.1	0.9	912.0
	11	100.0	65.0	55.0	8.8	1.0	69.2
	12	93.3	41.7	15.0	0.0	0.1	0.0
	13	100.0	60.0	56.2	9.5	0.9	10.5
	14	65.8	45.0	37.5	1.6	0.2	3801.9
	Mean	90.4 ± 17.6	52.7 ± 12.2	38.2 ± 22.0	4.0 ± 5.9		

For the participants without motor impairments, we obtain test classification accuracies between 40–65% with a mean of $54 \pm 7\%$. Since we have four mental tasks, a random classifier would be expected to achieve a classification accuracy of only 25%. A t-test leads us to believe that our mean classification accuracy is significantly better than chance ($p = 1.8\times10^{-5}$). A non-parametric Wilcoxon Signed Ranks test agrees with this conclusion ($p = 8.9\times10^{-3}$). The information transfer rates for this group range from 2–15bpm with a mean of 9 ± 4bpm, indicating that every user in this group would be able to correctly issue at least some instructions to a BCI.

For the group of participants with motor impairments, classification accuracy ranges from 15–56% with a mean of $38 \pm 22\%$. Among these participants, both a t-test ($p = 0.17$) and a

Wilcoxon test ($p = 0.19$) fail to conclude that our mean classification accuracy is better than chance; however, these tests have less statistical power for this smaller group of participants. The information transfer rates for this group range from 0–10bpm with a mean of 4 ± 6bpm. Upon close inspection, it appears that these information transfer rates may have a bimodal distribution across participants; although Participants 10, 12 and 14 are able to attain little or no information transfer, Participants 11 and 13 perform better than many of the participants without motor impairments.

A comparison of the performance between the two groups leads to borderline results. A two-sample, two-tailed t-test does not allow us to conclude a statistically significant difference in mean classification accuracy between the participants with impairments and those without impairments ($p = 0.12$). Similarly, a Mann-Whitney test, which may be more appropriate if the results have a bimodal distribution, also does not allow us to conclude with a high degree of certainty that there is a difference in mean classification accuracy between the groups ($p = 0.094$). However, the borderline p-values obtained from these tests and our observations about the performance of individual participants appears to be consistent with the notion that fewer people with impairments in home environments would be able to achieve an acceptable level of performance.

Table 4: Four-task test confusion matrix for Participant 1.

		Predicted (%)			
		Count	Fist	Rotate	Song
Actual (%)	Count	100	0	0	0
	Fist	50	30	10	10
	Rotate	0	10	60	30
	Song	20	20	0	60

Next, we seek to gain further insight into the types of misclassifications made by our algorithm by examining confusion matrices. In Table 4, we display the confusion matrix of test classification accuracies for Participant 1. In this instance, we note that the error rates and types are different for each mental task. For example, EEG segments that were recorded during the *count* task are never mislabeled as another task, i.e., there are zero false-negatives. However, EEG segments recorded during the *fist* and *song* tasks are incorrectly labeled as the *count* task, i.e., false positives, for 50% and 20% of segments, respectively.

Although individual confusion matrices can reveal the types of errors that occur for each participant, we are also interested in discovering which, if any, mental tasks perform well in general. One approach to answering this question is to examine the average confusion matrix for a number of participants that achieve high classification accuracy. In Table 5, we show the mean classification accuracies and 95% confidence intervals obtained by averaging the test confusion matrices for all participants that achieve a test classification accuracy of 50% or greater, i.e., Participants 1, 3, 4, 6, 8, 9, 11 and 13. Although the *count* task appears to have a relatively low false positive rate, none of the other mental tasks clearly stands out as being advantageous. Furthermore, the mean classification accuracy is roughly the same for each of the four mental tasks and the variability across each cell of the confusion matrices is relatively high. These observations suggest that the best-performing mental tasks vary considerably among participants.

Table 5: Four-task test confusion matrix averaged across participants that achieve at least 50% test classification accuracy.

		Predicted (%)			
		Count	Fist	Rotate	Song
Actual (%)	Count	65 ± 27	11 ± 8	11 ± 12	14 ± 15
	Fist	15 ± 22	55 ± 20	21 ± 17	9 ± 5
	Rotate	3 ± 4	15 ± 13	52 ± 12	30 ± 12
	Song	8 ± 7	12 ± 11	22 ± 17	58 ± 20

Assuming that the best-performing mental tasks are user-specific, or perhaps even session-specific, it seems appropriate for a BCI to select, during the calibration phase, which mental tasks should be used. Next, we explore this possibility by performing two-task classification using only the two tasks that achieved the highest classification accuracy in the averaged confusion matrix found during the validation procedure for each participant. Once the appropriate tasks are selected, new regularization parameters are found and the classifier is re-trained. Although using only the diagonal of the confusion matrix may not yield the best possible combination of mental tasks, this approach is more practical for use in real-time systems than an exhaustive search. Since only validation performance is used, this procedure avoids biasing our test results and could conceivably be used during BCI training.

Table 6: Two-task performance results.

	Participant	Training CA (%)	Validation CA (%)	Test CA (%)	Test ITR (bpm)	λ	γ	Task 1	Task 2
No Impairment	1	100.0	90.0	75.0	5.7	1.0	144.5	Count	Song
	2	100.0	90.0	80.0	8.3	0.4	3.6	Song	Count
	3	100.0	86.7	90.0	15.9	0.1	2.1	Song	Fist
	4	100.0	93.3	95.0	21.4	0.2	0.7	Rotate	Fist
	5	100.0	80.0	65.0	2.0	1.0	0.0	Count	Rotate
	6	100.0	96.7	95.0	21.4	1.0	0.5	Count	Song
	7	100.0	96.7	70.0	3.6	0.9	63.1	Fist	Song
	8	100.0	96.7	90.0	15.9	1.0	52.5	Fist	Rotate
	9	100.0	95.0	75.0	5.7	0.1	0.0	Count	Fist
	Mean	100.0 ± 0.0	91.7 ± 4.3	81.7 ± 8.6	11.1 ± 5.9				
Impairment	10	100.0	80.0	40.0	0.0	1.0	0.5	Count	Fist
	11	100.0	90.0	70.0	3.6	0.9	14.5	Rotate	Fist
	12	90.0	80.0	50.0	0.0	0.1	0.0	Rotate	Fist
	13	100.0	95.0	87.5	13.7	1.0	11.0	Song	Rotate
	14	94.2	90.0	60.0	0.9	0.2	218.8	Song	Count
	Mean	96.8 ± 5.7	87.0 ± 8.3	61.5 ± 22.8	3.6 ± 7.2				

In Table 6, we present the outcomes of these two-task experiments along with the tasks that were selected for each participant. For the group of participants without motor impairments,

we achieve test classification accuracies between 65–95% with a mean of $82 \pm 9\%$. Since we now have two classes, a random classifier would be expected to achieve 50% classification accuracy. A t-test confirms that our mean classification accuracy is significantly better than chance ($p = 2.8 \times 10^{-5}$) as does a Wilcoxon test ($p = 9.0 \times 10^{-3}$). The information transfer rates for this group range from 2–21bpm with a mean of 11 ± 6bpm. This suggests that all users in this group would be able to correctly issue at least some instructions to a BCI using only the two selected mental tasks.

For the group of participants with motor impairments, our two-task experiments result in classification accuracies ranging from 40–88% with a mean of $62 \pm 23\%$. For this smaller group of participants, we are again unable to demonstrate that the mean classification accuracy is better than chance using a t-test ($p = 0.23$) or Wilcoxon test ($p = 0.27$). The information transfer rates for this group range from 0–14bpm with a mean of 4 ± 7bpm. We also notice that the distribution of the information transfer rates has a bimodal appearance with the same three participants performing well in both the two-task and four-task scenarios.

For our two-task scenario, a comparison of the performance between the participants with and without motor impairments again yields borderline results. Although a two-sample t-test does not allow us to conclude with certainty that there is a difference in mean classification accuracy ($p = 0.069$), the non-parametric Mann-Whitney test does allow us to conclude a statistically significant difference ($p = 0.038$). The results of these tests appear to suggest that fewer participants with motor impairments would be able to achieve acceptable levels of performance in our two-task scenario; although a larger group of participants is likely required in order to draw firm conclusions. It is important to note, however, that one participant with motor impairments performed quite well, achieving about 88% classification accuracy with a 14bpm information transfer rate.

When comparing the difference in performance between the two-task and four-task scenarios, we first notice that there is a relatively large difference in classification accuracy between the two scenarios. For the participants without motor impairments a t-test ($p = 4.6 \times 10^{-5}$) and a Mann-Whitney test (4.6×10^{-4}) confirm that there is a statistically significant difference in mean classification accuracy between the two scenarios. For the group of participants with motor impairments, however, a t-test ($p = 0.08$) and Mann-Whitney test ($p = 0.095$) do not allow us to conclude a statistically significant difference in mean classification accuracy; although the results are somewhat borderline. An examination of the information transfer rates, however, reveals that there is very little difference in the amount of information that a BCI user would be able to communicate in either scenario. In other words, the two-task scenario might yield a BCI that makes fewer errors but the amount of work that a BCI user could accomplish is roughly the same.

6 Conclusions

In the present work, we have described a method for constructing forecasting models of EEG using ESN. These models may be advantageous over other approaches because of their ability to capture non-linear spatiotemporal patterns, their ability to be regularized and due to their computational efficiency. The recurrent architecture of ESN also makes them natural fit for modeling the transient oscillatory dynamics that are characteristic of EEG.

Using the configuration and parameter selection methods that we have outlined, we were able to produce ESN that forecast EEG well, achieving error rates as low as 3% of the signal range. Through iterated models, we were also able to show that ESN are capable of capturing

sophisticated patterns in EEG and that long-term, high-frequency and non-stationary patterns are more prevalent in models that have a large spectral radius. We believe that these models show considerable potential for capturing patterns in EEG and that they may have a number of potential applications in BCI as well as broader EEG analysis.

We then proposed a straightforward generative classification algorithm that uses these forecasting models to label EEG in the context of mental-task BCI. This approach uses a separate ESN for each mental task and assigns class labels according to the network that produces the lowest forecasting error. We tested this classifier in an offline fashion on EEG recorded using a portable eight-channel system from both participants without motor impairments in our laboratory as well as participants with severe motor impairments in their home environments. To our knowledge, we are the first to conduct experiments with mental-task BCI using EEG recorded from participants with motor impairments in their home environments.

When using all four mental tasks, we achieved information transfer rates between 2–15bpm for participants without motor impairments and 0–10bpm for participants with motor impairments. We also observed that the mean classification accuracy for participants without motor impairments was significantly higher than random and that the mean classification accuracy for participants with motor impairments was borderline higher than random. Additionally, it appears that the distribution of classification performance is somewhat bimodal, with some participants performing quite well and others performing near random. These observations lead us to two general conclusions. First, achieving consistently good results is more difficult under realistic conditions. Second, it appears that some users with impairments may be able to use such a BCI while others are may be unable to achieve an acceptable level of control.

We suspect that a combination of several factors is likely responsible for the differences in performance among the participants with impairments. First, we observed considerably more distraction in home environments than in our laboratory. For example, phones, pets and visitors are frequent causes of distraction. Second, EEG sensor displacement can be a problem. For instance, wheelchair headrests can make it difficult to maintain a good sensor-to-scalp connection following weight-shifts or other movements. Third, electrical interference is typically more prominent in home environments. In one case, a source of strong 60Hz interference was identified as a hospital bed and the interference was not eliminated until the bed was unplugged from the outlet. Finally, the various diseases and traumas that cause motor impairments could, potentially, have an adverse effect on the EEG signals utilized by a BCI. Unfortunately, the influence of disease and trauma on EEG has not been well-characterized. Clearly, future BCI research should consider these issues and focus on methods that are robust in real-world environments.

Although we obtained encouraging information transfer rates using four mental tasks, the corresponding error rates were relatively high. This would likely lead to a level of frustration for a user of an interactive BCI. In order to address this concern, we also explored the use of two mental tasks, which were selected during the validation procedure. In this two-task scenario, we achieved information transfer rates between 2–21bpm for the participants without motor impairments and between 0–14bpm for the participants with motor impairments. Again, we observed that the mean classification accuracy for participants without impairments was better than random and the mean classification accuracy for participants with impairments was borderline higher than random. We also again noted a bimodal distribution of performance across participants with one participant with a motor impairment achieving an information transfer rate of 14bpm. This suggests that some users may be able to use such a BCI under realistic conditions.

Although the information transfer rates we observed were not significantly different between the two and four-task scenarios, mean classification accuracy was significantly higher for the

participants without impairments in the two-task scenario. This leads us to conclude that while the two and four task scenarios would allow a BCI user to accomplish about the same amount of work, the two-task scenario would lead to a lower error rate. Although a lower error rate may be less frustrating for a BCI user, these gains come at the expense of fewer degrees of control.

In the present work, we have not directly compared our approach to other classification algorithms. However, a review of current literature on mental-task BCI along with our estimate of information transfer rate, computed using (11), suggests that offline performance ranges from about 3–41bpm among state-of-the-art algorithms [7, 9, 12, 19, 20]. It is important to note, however, that the results at the high end of this range typically achieve moderate classification accuracies with high information transfer rates because they assign class labels at intervals of less than one second. These studies also only involve participants without motor impairments in laboratory environments and typically use EEG acquisition systems with more channels and higher sampling rates than the portable system used in the present work. In one study, however, Millán, et al., performed online classification using a portable EEG system at a rate of about 2–80bpm after several consecutive days of training with feedback [20]. Although more comparative work is clearly required, this review leads us to believe that our classification algorithm performs on par with approaches that have been evaluated in offline settings and that training with feedback may have the potential to improve performance considerably.

In our previous work, we explored a classifier that was similar to the approach described in the present manuscript except that it used Elman Recurrent Neural Networks (ERNN) instead of ESN [15, 16]. In these works, we observed information transfer rates between 0–38bpm with decisions made at one-second intervals for two participants without impairments and three participants with severe motor impairments using a non-portable EEG system. Although we observed a higher peak performance for ERNN, at least for some individuals, it is presently intractable to train and perform parameter selection for ERNN in a real-time BCI. Therefore, a primary advantage of ESN over ERNN is computational efficiency. However, a thorough comparison between these two approaches is required in order to draw firm conclusions.

We believe that the next step in this line of research should be to explore modeling EEG at multiple time-scales through multi-step predictions and iterated models. It is also important to perform direct comparisons with other time-series models and classifiers in order to precisely quantify the advantages and disadvantages of these approaches. Additionally, we suspect that more carefully designed filtering and artifact removal algorithms may lead to better performance under realistic conditions. Finally, we feel that it is important to conduct interactive experiments. Since the ability to control computerized devices is the final goal of assistive BCI and because users may learn to improve performance in the presence of feedback, real-time experiments should be a focal point of future BCI research.

References

[1] Luis Nicolas-Alonso and Jaime Gomez-Gil. Brain computer interfaces, a review. *Sensors*, 12(2):1211–1279, 2012.

[2] Jean-Dominique Bauby. *The diving bell and the butterfly: A memoir of life in death*. Vintage, 1998.

[3] Eric Sellers, Theresa Vaughan, and Jonathan Wolpaw. A brain-computer interface for long-term independent home use. *Amyotrophic lateral sclerosis*, 11(5):449–455, 2010.

[4] Guido Dornhege. *Toward brain-computer interfacing*. The MIT Press, 2007.

[5] Jonathan Wolpaw and Elizabeth Winter Wolpaw. *Brain-computer interfaces: principles and practice*. Oxfort University Press, 2012.

[6] Paul Nunez and Ramesh Srinivasan. *Electric fields of the brain: the neurophysics of EEG*. Oxford University Press, USA, 2006.

[7] Zachary Keirn and Jorge Aunon. A new mode of communication between man and his surroundings. *IEEE Transactions on Biomedical Engineering*, 37(12):1209–1214, 1990.

[8] Charles Anderson, Erik Stolz, and Sanyogita Shamsunder. Discriminating mental tasks using EEG represented by AR models. In *17th Annual Conference of The IEEE Engineering in Medicine and Biology Society*, volume 2, pages 875–876. IEEE, 1995.

[9] Charles Anderson, Erik Stolz, and Sanyogita Shamsunder. Multivariate autoregressive models for classification of spontaneous electroencephalographic signals during mental tasks. *IEEE Transactions on Biomedical Engineering*, 45(3):277–286, 1998.

[10] Charles Anderson, James Knight, Tim O'Connor, Michael Kirby, and Artem Sokolov. Geometric subspace methods and time-delay embedding for EEG artifact removal and classification. *IEEE Transactions on Neural Systems and Rehabilitation Engineering*, 14(2):142–146, 2006.

[11] Charles Anderson, James Knight, Michael Kirby, and Douglas Hundley. Classification of time-embedded EEG using short-time principal component analysis. *Toward Brain-Computer Interfacing*, pages 261–278, 2007.

[12] Charles Anderson and Jeshua Bratman. Translating thoughts into actions by finding patterns in brainwaves. In *Proceedings of the Fourteenth Yale Workshop on Adaptive and Learning Systems*, pages 1–6, 2008.

[13] Charles Anderson, Elliott Forney, Douglas Hains, and Annamalai Natarajan. Reliable identification of mental tasks using time-embedded EEG and sequential evidence accumulation. *Journal of Neural Engineering*, 8(2):025023, 2011.

[14] Damien Coyle, Girijesh Prasad, and Thomas McGinnity. A time-series prediction approach for feature extraction in a brain-computer interface. *IEEE Transactions on Neural Systems and Rehabilitation Engineering*, 13(4):461–467, 2005.

[15] Elliott Forney and Charles Anderson. Classification of EEG during imagined mental tasks by forecasting with elman recurrent neural networks. *International Joint Conference on Neural Networks (IJCNN)*, pages 2749–2755, 2011.

[16] Elliott Forney. Electroencephalogram classification by forecasting with recurrent neural networks. Master's thesis, Department of Computer Science, Colorado State University, Fort Collins, CO, 2011.

[17] Elliott Forney, Charles Anderson, William Gavin, and Patricia Davies. A stimulus-free brain-computer interface using mental tasks and echo state networks. In *Proceedings of the Fifth International Brain-Computer Interface Meeting: Defining the Future*. Graz University of Technology Publishing House, 2013.

[18] Elisabeth Friedrich, Reinhold Scherer, and Christa Neuper. The effect of distinct mental strategies on classification performance for brain–computer interfaces. *International Journal of Psychophysiology*, 84(1):86–94, 2012.

[19] Elisabeth Friedrich, Reinhold Scherer, and Christa Neuper. Long-term evaluation of a 4-class imagery-based brain–computer interface. *Clinical Neurophysiology*, 2013.

[20] José Millán, Josep Mouriño, Marco Franzé, Febo Cincotti, Markus Varsta, Jukka Heikkonen, and Fabio Babiloni. A local neural classifier for the recognition of EEG patterns associated to mental tasks. *IEEE Transactions on Neural Networks*, 13(3):678–686, 2002.

[21] José Millán, Frédéric Renkens, Josep Mouriño, and Wulfram Gerstner. Brain-actuated interaction. *Artificial Intelligence*, 159(1):241–259, 2004.

[22] José Millán, Pierre Ferrez, Ferran Galán, Eileen Lew, and Ricardo Chavarriaga. Non-invasive brain-machine interaction. *International Journal of Pattern Recognition and Artificial Intelligence*, 22(05):959–972, 2008.

[23] Ferran Galán, Marnix Nuttin, Eileen Lew, Pierre Ferrez, Gerolf Vanacker, Johan Philips, and José Millán. A brain-actuated wheelchair: Asynchronous and non-invasive brain-computer interfaces for continuous control of robots. *Clinical Neurophysiology*, 119(9):2159–2169, 2008.

[24] Li Zhiwei and Shen Minfen. Classification of mental task EEG signals using wavelet packet entropy and SVM. In *8th International Conference on Electronic Measurement and Instruments*, pages 3–906. IEEE, 2007.

[25] Gert Pfurtscheller. Event-related synchronization (ers): an electrophysiological correlate of cortical areas at rest. *Electroencephalography and clinical neurophysiology*, 83(1):62–69, 1992.

[26] Elisabeth Friedrich, Reinhold Scherer, and Christa Neuper. Do user-related factors of motor impaired and able-bodied participants correlate with classification accuracy? In *Proceedings of the 5th International Brain-Computer Interface Conference*, pages 156–159. Graz University of Technology, 2011.

[27] Zachary Cashero. Comparison of EEG preprocessing methods to improve the performance of the P300 speller. Master's thesis, Department of Computer Science, Colorado State University, Fort Collins, CO, 2011.

[28] Damien Coyle, Girijesh Prasad, and Thomas McGinnity. Extracting features for a brain-computer interface by self-organising fuzzy neural network-based time series prediction. In *26th Annual International Conference of The IEEE Engineering in Medicine and Biology Society*, volume 2, pages 4371–4374. IEEE, 2004.

[29] Damien Coyle, Thomas McGinnity, and Girijesh Prasad. Creating a nonparametric brain-computer interface with neural time-series prediction preprocessing. In *28th Annual International Conference of The IEEE Engineering in Medicine and Biology Society*, pages 2183–2186. IEEE, 2006.

[30] Damien Coyle, Thomas McGinnity, and Girijesh Prasad. A multi-class brain-computer interface with SOFNN-based prediction preprocessing. In *The 2008 International Joint Conference on Neural Networks (IJCNN)*, pages 3696–3703. IEEE, 2008.

[31] Vaibhav Gandhi, Vipul Arora, Laxmidhar Behera, Girijesh Prasad, Damien Coyle, and Thomas McGinnity. EEG denoising with a recurrent quantum neural network for a brain-computer interface. In *The 2011 International Joint Conference on Neural Networks (IJCNN)*, pages 1583–1590. IEEE, 2011.

[32] Vaibhav Gandhi, Girijesh Prasad, Damien Coyle, Laxmidhar Behera, and Thomas McGinnity. Quantum neural network-based EEG filtering for a brain-computer interface. *IEEE Transactions on Neural Networks and Learning Systems*, 25(2):278–288, 2014.

[33] Herbert Jaeger. Tutorial on training recurrent neural networks, covering BPTT, RTRL, EKF and the echo state network approach. *GMD Report 159: German National Research Center for Information Technology*, 2002.

[34] Herbert Jaeger. Adaptive nonlinear system identification with echo state networks. In *Advances in Neural Information Processing Systems (Proceedings of NIPS 15)*, volume 15, pages 593–600. MIT Press, 2003.

[35] Herbert Jaeger and Harald Haas. Harnessing nonlinearity: Predicting chaotic systems and saving energy in wireless communication. *Science*, 304(5667):78–80, 2004.

[36] Elliott Forney, Charles Anderson, Patricia Davies, William Gavin, Brittany Taylor, and Marla Roll. A comparison of EEG systems for use in P300 spellers by users with motor impairments in real-world environments. In *Proceedings of the Fifth International Brain-Computer Interface Meeting: Defining the Future*. Graz University of Technology Publishing House, 2013.

[37] William Gavin and Patricia Davies. Obtaining reliable psychophysiological data with child participants. *Developmental Psychophysiology: Theory, Systems, and Methods. Cambridge University Press, New York, NY*, pages 424–447, 2008.

[38] College of Health and Human Sciences at Colorado State University. Brainwaves research laboratory. `http://brainwaves.colostate.edu`, Oct 2015.

[39] Department of Compter Science at Colorado State University. CEBL: CSU EEG and Brain-Computer Interface Laboratory. `http://www.cs.colostate.edu/eeg/main/software/cebl3`, Oct 2015.

[40] Fraunhofer Institute for Intelligent Analysis and Information Systems. International Patent No. WO/2002/031764, 2002.

[41] Jonathan Wolpaw, Herbert Ramoser, Dennis McFarland, and Gert Pfurtscheller. EEG-based communication: improved accuracy by response verification. *IEEE Transactions on Rehabilitation Engineering*, 6(3):326–333, 1998.

[42] John Pierce. *An introduction to information theory: symbols, signals & noise*. Dover, 1980.